Bulletin of the Seismological Society of America, Vol. 89, No. 1, pp. 54–68, February 1999

# 3D Elastic Finite-Difference Modeling of Seismic Motion Using Staggered Grids with Nonuniform Spacing

by Arben Pitarka

**Abstract** This article provides a technique to model seismic motions in 3D elastic media using fourth-order staggered-grid finite-difference (FD) operators implemented on a mesh with nonuniform grid spacing. The accuracy of the proposed technique has been tested through comparisons with analytical solutions, conventional 3D staggered-grid FD with uniform grid spacing, and reflectivity methods for a variety of velocity models. Numerical tests with nonuniform grids suggest that the method allows sufficiently accurate modeling when the grid sampling rate is at least 6 grid points per shortest shear wavelength. The applicability for a finite fault with nonuniform distribution of point sources is also confirmed. The use of nonuniform spacing improves the efficiency of the FD methods when applied to large-scale structures by partially avoiding the spatial oversampling introduced by the uniform spacing in zones with high velocity. The significant reduction in computer memory that can be obtained by the new technique improves the efficiency of the 3D-FD method at handling shorter wavelengths, larger areas, or more realistic 3D velocity structures.

## Introduction

Studies of wave propagation and strong-ground-motion simulation based on three-dimensional finite-difference (3D-FD) methods have contributed to a better understanding of the source process, wave-path effects, and basin structure response (e.g., Miyatake, 1980; Frankel and Vidale, 1992; Frankel, 1993; Graves, 1993; Yomogida and Etgen, 1993; Olsen *et al.,* 1995; Olsen and Archuleta, 1996; Graves, 1996a; Pitarka and Irikura, 1996; Ohminato and Chouet, 1997; Pitarka *et al.,* 1998; Wald and Graves, 1998; Graves, 1998).

In order to handle the tremendous computational and storage requirements that are inherent to the 3D-FD technique, a variety of computational approaches have been developed and implemented. Some researchers have addressed these computational demands by designing the codes to run on supercomputer platforms that contain a large number of parallel processors (e.g., Olsen *et al.,* 1995). The main drawbacks to this approach are that these types of machines are not commonly available and that the CPU time can be very expensive. A significant improvement of the 3D-FD method is achieved by the application of the memory optimization algorithm, presented by Graves (1996b), which allows large-scale 3D-FD problems to be computed on a conventional, single-processor desktop workstation. In this algorithm, model storage is accommodated using both external (hard disk) and internal (core) memory. The transfer of data between the storage devices is done with an efficient time update algorithm that maximizes the number of computations performed between successive I/O operations. This cascaded approach reduces system overhead to less than a few percent of the total computation time (Graves, 1998).

A common feature of the 3D-FD techniques previously discussed is the use of the uniform-grid formulation (i.e., constant grid spacing), which requires relatively large computer memory. Due to computational limitations, these studies have been restricted to long periods (usually longer than 1 sec) and have used relatively high values for the shear velocity of near-surface sediments in many cases. The development of 3D-FD techniques that can model shorter period ground motion using realistic velocity structures without requiring additional computer memory has therefore become a primary goal for the continuing progress of numerical simulation techniques.

The most efficient grid for reducing computer memory requirements is obtained by assembling grids with different spacing that cover different regions of the model. The interaction between regions is realized through interpolations of the field variable in the areas where the grid is discontinuous. The technique has been initially applied for modeling wave propagation in 2D media (Yuan *et al.,* 1986; Jastram and Behle, 1992; Jastram and Tessmer, 1994; Falk *et al.,* 1996) and later extended to 3D elastic media (Aoi and Fujiwara, 1997) by using a vertically discontinuous grid. The technique has not been fully generalized for treating grids with spacing that is discontinuous in three directions. Further work is needed to investigate the transparency of the bound-

aries between grids, which involves interpolation of the wave field on more than one plane, including the ones that reach the free surface. Special FD formulas are used for points at the contact of the two grids in Moczo *et al.* (1996).

There are attractive ways of avoiding the wave-field interpolation required in the above-mentioned finite-difference schemes to use the finite-element method in the transition zone (Moczo *et al.*, 1997) and to use finite-difference operators that are suitable for grids with nonuniform spacing. Miyatake (1980) proposed a finite-difference operator that can be used in the conventional finite-difference scheme with nonuniform grid spacing to solve the wave equation in 3D elastic media. A different approach was used by Moczo (1989), who proposed an efficient finite-difference technique for treating *SH* waves in 2D media using grids with nonuniform spacing. Both schemes are based on finite-difference operators of second-order accuracy for the first and second derivatives of the field variable appearing in the wave equation. The corresponding explicit fourth-order expressions for conventional finite-difference schemes are much more complicated. They have been derived by Mufti *et al.* (1996), who used the Lagrange polynomial method and *Mathematica*, an algebraic manipulation software package.

In this article, I develop fourth-order expressions for discrete spatial differential operators in the staggered-grid 3D-FD formulation that are designed for rectangular grids with nonuniform grid spacing (Fig. 1). By applying these operators, we are able to partially adapt the grid spacing to the velocity structure in accordance with the accuracy condition required by the finite-difference method. The use of nonuniform grid spacing improves the efficiency of the finite-difference methods when applied to large-scale structures by avoiding the spatial oversampling introduced by the constant grid spacing in zones with high velocity. The significant reduction in computer memory requirement obtained by the present technique improves the efficiency of the 3D FD in handling shorter wavelengths, larger areas, or more realistic 3D velocity structures.

In the following sections, I provide detailed formulations of the discrete spatial differential operators and show the performance of the proposed technique based on some numerical tests.

## Finite-Difference Operators for the Rectangular Grid with Nonuniform Spacing

To model wave propagations in 3D elastic media, I basically follow the staggered-grid finite-difference method proposed by Virieux (1986), Levander (1988), and Graves (1996b), which solves the following elastodynamic equations:

$$\begin{aligned}
\partial_t v_x &= b(\partial_x \tau_{xx} + \partial_y \tau_{xy} + \partial_z \tau_{xz}) + f_x,\\
\partial_t v_y &= b(\partial_x \tau_{xy} + \partial_y \tau_{yy} + \partial_z \tau_{yz}) + f_y,\\
\partial_t v_z &= b(\partial_x \tau_{xz} + \partial_y \tau_{yz} + \partial_z \tau_{zz}) + f_z,
\end{aligned}$$

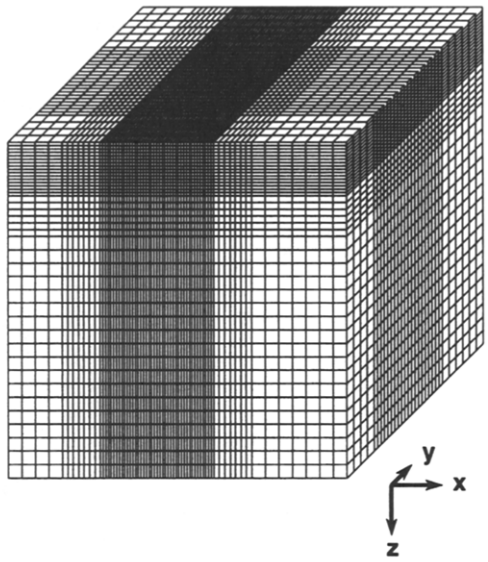


Figure 1. Grid layout with nonuniform spacing.

$$\begin{aligned}
\partial_t \tau_{xx} &= (\lambda + 2\mu)\partial_x v_x + \lambda(\partial_y v_y + \partial_z v_z),\\
\partial_t \tau_{yy} &= (\lambda + 2\mu)\partial_y v_y + \lambda(\partial_x v_x + \partial_z v_z),\\
\partial_t \tau_{zz} &= (\lambda + 2\mu)\partial_z v_z + \lambda(\partial_x v_x + \partial_y v_y),\\
\partial_t \tau_{xy} &= \mu(\partial_y v_x + \partial_x v_y),\\
\partial_t \tau_{xz} &= \mu(\partial_z v_x + \partial_x v_z),\\
\partial_t \tau_{yz} &= \mu(\partial_z v_y + \partial_y v_z).
\end{aligned} \tag{1}$$

Here, $(v_x,v_y,v_z)$ are the particle velocity components; $(\tau_{xx},\tau_{yy},\tau_{zz},\tau_{xy},\tau_{xz},\tau_{yz})$ are the stress components; $(f_x,f_y,f_z)$ are the body-force components; $b$ is the buoyancy; $\lambda$ and $\mu$ are Lame's coefficients; and $\partial_x,\partial_y,\partial_z$, and $\partial_t$ represent the partial differential operators $\partial/\partial_x$, $\partial/\partial_y$, $\partial/\partial_z$, and $\partial/\partial_t$, respectively.

The staggered grid defines some of the velocity and stress components shifted from the locations of other components by half the grid length in space (Fig. 2). By using second-order approximation for time derivatives, the solution of equations (1) can be expressed in a discrete form by

$$\begin{aligned}
v_x^{n+1/2}{}_{i,j,k} &= v_x^{n-1/2}{}_{i,j,k} + \Delta t b_x (D_x \tau_{xx}\\
&\quad + D_y \tau_{xy} + D_z \tau_{xz})|^n{}_{i,j,k},\\
v_y^{n+1/2}{}_{i+1/2,j+1/2,k} &= v_y^{n-1/2}{}_{i+1/2,j+1/2,k} + \Delta t b_y (D_x \tau_{xy}\\
&\quad + D_y \tau_{yy} + D_z \tau_{yz})|^n{}_{i+1/2,j+1/2,k},\\
v_z^{n+1/2}{}_{i+1/2,j,k+1/2} &= v_z^{n-1/2}{}_{i+1/2,j,k+1/2} + \Delta t b_z (D_x \tau_{xz}\\
&\quad + D_y \tau_{yz} + D_z \tau_{zz})|^n{}_{i+1/2,j,k+1/2},
\end{aligned}$$

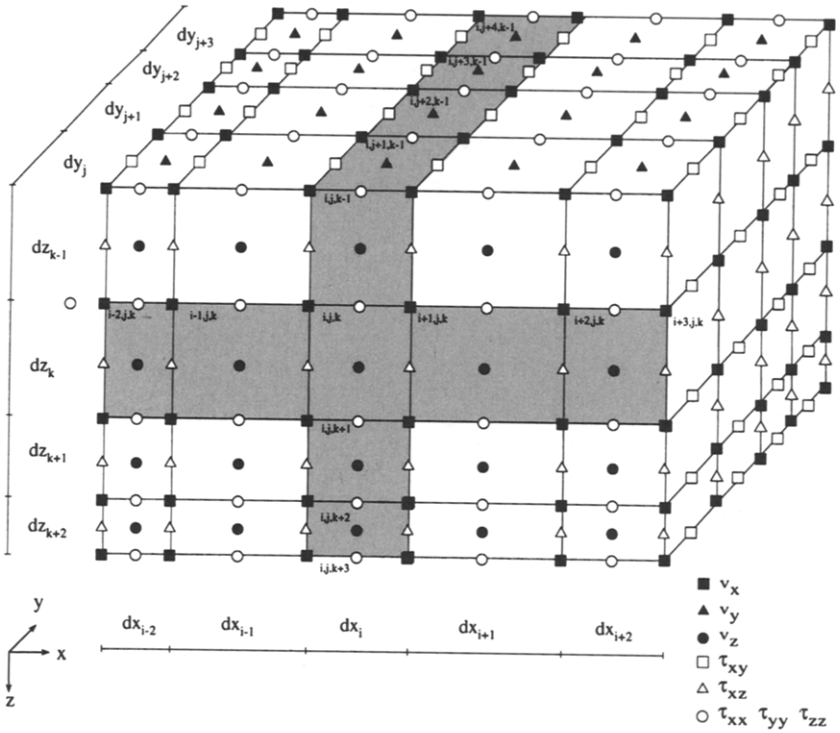


Figure 2. Schematic representation of unit cells with the grid spacing ($dx_i$,$dy_j$,$dz_k$) variable in $x$, $y$, and $z$ directions. The indices $i,j,k$ represent grid coordinates.

$$\tau_{xx}{}^{n+1}_{i+1/2,j,k} = \tau^n_{xx\ i+1/2,j,k} + \Delta t[(\lambda + 2\mu)D_x v_x + \lambda(D_y v_y + D_z v_z)]|^{n+1/2}_{i+1/2,j,k},$$

$$\tau_{yy}{}^{n+1}_{i+1/2,j,k} = \tau^n_{yy\ i+1/2,j,k} + \Delta t[(\lambda + 2\mu)D_y v_y + \lambda\,(D_x v_x + D_z v_z)]|^{n+1/2}_{i+1/2,j,k}, \quad (2)$$

$$\tau_{zz}{}^{n+1}_{i+1/2,j,k} = \tau^n_{zz\ i+1/2,j,k} + \Delta t[(\lambda + 2\mu)D_z v_z + \lambda\,(D_x v_x + D_y v_y)]|^{n+1/2}_{i+1/2,j,k},$$

$$\tau_{xy}{}^{n+1}_{i,j+1/2,k} = \tau^n_{xy\ i,j+1/2,k} + \Delta t[\mu_{xy}(D_y v_x + D_x v_y)]|^{n+1/2}_{i,j+1/2,k},$$

$$\tau_{xz}{}^{n+1}_{i,j,k+1/2} = \tau^n_{xz\ i,j,k+1/2} + \Delta t[\mu_{xz}(D_z v_x + D_x v_z)]|^{n+1/2}_{i,j,k+1/2},$$

$$\tau_{yz}{}^{n+1}_{i+1/2,j+1/2,k+1/2} = \tau^n_{yz\ i+1/2j+1/2,k+1/2} + \Delta t[\mu_{yz}(D_z v_y + D_y v_z)]|^{n+1/2}_{i,j,k+1/2},$$

In these equations, the superscripts refer to the time index, and the subscripts refer to the spatial indices. $\Delta t$ is the time step and $D_x$, $D_y$, and $D_z$ represent the central finite-difference operators of the spatial derivatives $\partial_x$, $\partial_y$, and $\partial_z$, respectively. I use effective parameters for the buoyancy $b$ and the rigidity $\mu$ suggested by Graves (1996b):

$$b_x = 0.5(b_{i,j,k} + b_{i+1,j,k}),$$

$$b_y = 0.5(b_{i,j,k} + b_{i,j+1,k}),$$

$$b_z = 0.5(b_{i,j,k} + b_{i,j,k+1}),$$

$$\mu_{xy} = [0.25(1/\mu_{i,j,k} + 1/\mu_{i+1,j,k} + 1/\mu_{i,j+1,k} + 1/\mu_{i+1,j+1,k})]^{-1},$$

$$\mu_{xz} = [0.25(1/\mu_{i,j,k} + 1/\mu_{i+1,j,k} + 1/\mu_{i,j,k+1} + 1/\mu_{i+1,j,k+1})]^{-1},$$

$$\mu_{yz} = [0.25(1/\mu_{i,j,k} + 1/\mu_{i,j+1,k} + 1/\mu_{i,j,k+1} + 1/\mu_{i,j+1,k+1})]^{-1}.$$

Suppose that the field variable $g$ represents one component of particle velocity ($v_x$,$v_y$,$v_z$) or stress tensor ($\tau_{xx}$,$\tau_{yy}$,$\tau_{zz}$,$\tau_{xy}$,$\tau_{xz}$,$\tau_{yz}$). The fourth-order finite-difference operator with respect to $x$ acting on a field variable $g$ can be expressed by the equation

$$D_x g(x,y,z) = c_1 g(x + \Delta_1,y,z) + c_2 g(x - \Delta_2,y,z) + c_3 g(x + \Delta_3,y,z) + c_4 g(x - \Delta_4,y,z), \quad (3)$$

where $c_i$ are four coefficients to be determined. Spatial increments $\Delta_i$ can be expressed in terms of the variable grid spacing $dx$. $\Delta_i$ are schematically shown in Figure 3. Similar

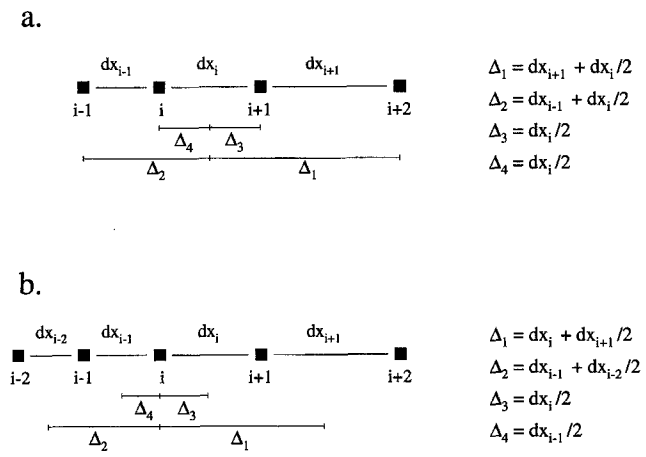


Figure 3. Grid nodes with nonuniform spacing in the $x$ direction. $\Delta_i$ ($i$ = 1,4) are used to calculate the finite-difference operator $D_x$ centered between (a) the nodes $i$ and $i$ + 1 and (b) that centered at the node $i$.

equations can be used to express the finite-difference operators $D_y$ and $D_z$.

Because I am considering the spatial derivative of the variable $g$ with respect to $x$, I assume $g(x,y,z) = g_{yz}\exp(ikx)$ with $g_{yz}$ representing its dependence only on $y$ and $z$. After replacing $g$ in (3), we obtain

$$ik = c_1\exp(+ik\Delta_1) + c_2\exp(-ik\Delta_2) + c_3\exp(+ik\Delta_3) + c_4\exp(-ik\Delta_4). \quad (4)$$

I use the Taylor's expansion up to order $O(\Delta_i^4)$ to approximate the exponentials in equation (4):

$$\exp(+ik\Delta_i) \approx (1 + ik\Delta_i - 1/2k^2\Delta_i^2 - ik^3/6\Delta_i^3). \quad (5)$$

After substituting equation (5) into (4) and rearranging, we obtain

$$\begin{aligned} ik = {} & (c_1 + c_2 + c_3 + c_4) \\ & + ik\,(c_1\Delta_1 - c_2\Delta_2 + c_3\Delta_3 - c_4\Delta_4) + \\ & + k^2/2\,(-c_1\Delta_1^2 - c_2\Delta_2^2 - c_3\Delta_3^2 - c_4\Delta_4^2) \\ & + ik^3/6\,(-c_1\Delta_1^3 + c_2\Delta_2^3 - c_3\Delta_3^3 + c_4\Delta_4^3). \end{aligned} \quad (6)$$

Equation (6) can be replaced by a system of four linear equations:

$$\begin{pmatrix} 1 & 1 & 1 & 1 \\ \Delta_1 & -\Delta_2 & +\Delta_3 & -\Delta_4 \\ -\Delta_1^2 & -\Delta_2^2 & -\Delta_3^2 & -\Delta_4^2 \\ -\Delta_1^3 & +\Delta_2^3 & -\Delta_3^3 & +\Delta_4^3 \end{pmatrix} \begin{pmatrix} c_1 \\ c_2 \\ c_3 \\ c_4 \end{pmatrix} = \begin{pmatrix} 0 \\ 1 \\ 0 \\ 0 \end{pmatrix}. \quad (7)$$

By solving the system (7), we find the coefficients $c_i$ of the fourth-order finite-difference operator $D_x$. Coefficients $c_i$ in the operators $D_y$ and $D_z$ are similarly determined.

For staggered grids, the finite-difference operators are expressed in terms of two different sets of coefficients $c_i$ that depend on the position of field variables (see Fig. 2). Expressions of $\Delta_i$ as functions of the variable grid spacing ($dx,dy,dz$) in the operators $D_x$, $D_y$, and $D_z$ are shown in Table 1.

The coefficients $c_i$ are generated prior to the finite-difference calculation, once the nonuniform grid is chosen, which in turn is based on the velocity distribution and the maximum frequency required in the modeling.

## Moment-Tensor Source Implementation

Here I present a moment-tensor source formulation that uses stress components instead of particle velocity components at the source (e.g., Coutant *et al.*, 1995). Compared to the velocity approach (e.g., Graves, 1996b), the stress approach is simpler and easy to implement in the grid with variable spacing. The moment-tensor source formulation uses equivalent body forces that are appropriately added every time step to each component of the stress tensor at the grid point corresponding to the source location. In our scheme, the source is colocated with the normal stress components $\tau_{ii}$. For example, stress components for a source located at the grid node $i$ + 1/2,$j$,$k$ are given by the following equations:

$$\begin{aligned} \tau^n_{xx\ i+1/2,j,k} &= \tau^n_{xx\ i+1/2,j,k} - \Delta t\dot{M}_{xx}(t)/V \\ \tau^n_{yy\ i+1/2,j,k} &= \tau^n_{yy\ i+1/2,j,k} - \Delta t\dot{M}_{yy}(t)/V \\ \tau^n_{zz\ i+1/2,j,k} &= \tau^n_{zz\ i+1/2,j,k} - \Delta t\dot{M}_{zz}(t)/V \\ \tau^n_{xz\ i,j,k+1/2} &= \tau^n_{xz\ i,j,k+1/2} - \Delta t\dot{M}_{xz}(t)/V \\ \tau^n_{xy\ i,j+1/2,k} &= \tau^n_{xy\ i,j+1/2,k} - \Delta t\dot{M}_{xy}(t)/V \\ \tau^n_{yz\ i+1/2,j+1/2,k+1/2} &= \tau^n_{yz\ i+1/2,j+1/2,k+1/2} - \Delta t\dot{M}_{yz}(t)/V \end{aligned} \quad (8)$$

$\dot{M}_{xx}(t)$, $\dot{M}_{yy}(t)$, $\dot{M}_{zz}(t)$, $\dot{M}_{xz}(t)$, $\dot{M}_{xy}(t)$, and $\dot{M}_{yz}(t)$ are the time derivatives of the moment-tensor components, proportional to the slip velocity function on the fault. $V$ is equal to the effective volume of the grid cell in the source area:

$$V = (dx_i + dx_{i-1})*(dy_j + dy_{j-1})*(dz_k + dz_{k-1})/8. \quad (9)$$

## Computational Requirements

The finite-difference computation based on the proposed scheme is performed in two steps. In the first step, two sets of four coefficients $c_i$ for each finite-difference operator $D_x$, $D_y$, and $D_z$ are generated. Note that the coefficients

Table 1
Expressions of $\Delta_i$ Used in the Calculation of the Finite-Difference Operators

| Finite-Difference Operator | $\Delta_1$ | $\Delta_2$ | $\Delta_3$ | $\Delta_4$ |
|---|---|---|---|---|
| $D_x$ acting on $v_z$, $v_y$, and $\tau_{xx}$ | $dx_{i+1} + dx_j/2$ | $dx_{i-1} + dx_i/2$ | $dx_i/2$ | $dx_i/2$ |
| $D_x$ acting on $v_x$, $\tau_{xy}$, and $\tau_{xz}$ | $dx_i + dx_{i+1}/2$ | $dx_{i-1} + dx_{i-2}/2$ | $dx_i/2$ | $dx_{i-1}/2$ |
| $D_y$ acting on $v_y$, $\tau_{xy}$, and $\tau_{yz}$ | $dy_{j+1} + dy_j/2$ | $dy_{j-1} + dy_j/2$ | $dy_j/2$ | $dy_j/2$ |
| $D_y$ acting on $v_z$, $v_x$, and $\tau_{yy}$ | $dy_j + dy_{j+1}/2$ | $dy_{j-1} + dy_{j-2}/2$ | $dy_j/2$ | $dy_{j-1}/2$ |
| $D_z$ acting on $v_z$, $\tau_{xz}$, and $\tau_{yz}$ | $dz_{k+1} + dz_k/2$ | $dz_{k-1} + dz_k/2$ | $dz_k/2$ | $dz_k/2$ |
| $D_z$ acting on $v_x$, $v_y$, and $\tau_{zz}$ | $dz_k + dz_{k+1}/2$ | $dz_{k-1} + dz_{k-2}/2$ | $dz_k/2$ | $dz_{k-1}/2$ |

of the finite-difference operator $D_x$ vary only in the $x$ direction. They are invariant in the $y$ and $z$ directions. If the whole system has $N_x$ grid cells in the $x$ direction, the total number of coefficients required for $D_x$ in the grid is $8*N_x$. In a similar manner, the total number of coefficients required for $D_y$ and $D_z$ is respectively $8*N_y$ and $8*N_z$. The total number of coefficients is

$$NC = 8*(N_x + N_y + N_z).$$

It is obvious that the computer core memory needed to store the $NC$ coefficients is much smaller than the memory saved by the application of this scheme. In the second step, the finite-difference scheme described by equation (2) is applied in the same fashion as the usual staggered-grid scheme with constant grid spacing. I use the zero-stress formulation of Graves (1996b) for the free surface and the A1 absorbing boundary condition of Clayton and Engquist (1977) for the other boundaries. The original A1 formulation is modified for the present variable grid spacing.

The maximum frequency of the seismic wave that can be accurately modeled by the proposed scheme is considered to by the minimum of all frequencies $f_{\text{cell}}$ calculated for each unit cell using the following condition:

$$f_{\text{cell}} < v_{\min}/5h,$$

where $h$ and $v_{\min}$ are the largest grid spacing and minimum wave speed, respectively, within each grid cell. This accuracy condition is determined through numerical tests.

A theoretical analysis of the stability condition of the proposed scheme is difficult to obtain. The usual approach to derive the stability condition of the staggered-grid scheme with constant grid spacing (e.g., Virieux, 1986; Levander, 1988) results in complicated algebraic operations when applied to the present scheme. Guided by the results of these earlier studies, and using a series of numerical tests, I found that the stability criterion for each unit cell is satisfied by

$$\Delta t_{\text{cell}} < 0.495\ h/v_{\max},$$

where $\Delta t_{\text{cell}}$, $h$, and $v_{\max}$ are the time increment, smallest grid spacing, and maximum wave speed, respectively, within

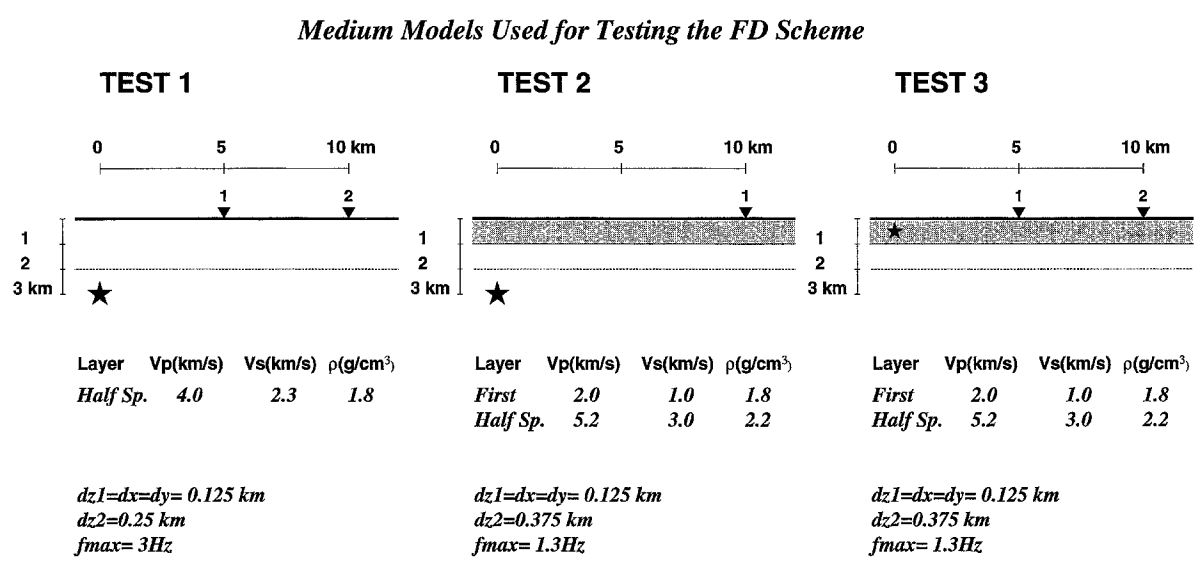


Figure 4. Three flat-layered models. The dotted line indicates the boundary between zones with different vertical grid spacing, and the star indicates the dislocation point source.

each cell. The stability criterion for the entire grid is satisfied when the time increment used in the calculation is the minimum of all $\Delta t_{cell}$.

## Performance of the Nonuniform-Grid Finite-Difference Operators

To assess the accuracy of the proposed finite-difference operators, I implemented them into the finite-difference scheme and performed several calculations to model the wave propagation in laterally homogeneous and heterogeneous media. Homogenous half-space (TEST1) and two-layered models (TEST2 and TEST3) along with station and source locations are shown in Figure 4. In the three tests, I calculated velocity seismograms for a double-couple point source with a focal mechanism of strike = 30°, dip = 80°, rake = 30°, and a bell-shaped source-time function $f(t) = [1 - \cos(2\pi t/T_0)]/T_0$ with a duration $T_0 = 1.0$ sec. The strike angle is measured with respect to the $y$ direction in the 3D grid.

With the model TEST1 (Fig. 4, left panel), I assumed $Vp$ = 4.0 km/sec, $Vs$ = 2.3 km/sec, $\rho$ = 1.8 g/cm$^3$, and a source depth 3 km, and I used two observation points on the free surface at horizontal ranges of 5 and 10 km, respectively. The purpose of the calculation was to test the accuracy of the proposed scheme when the vertical grid spacing increases abruptly from 0.125 to 0.25 km at the depth of 2 km. The grid spacing in the two horizontal directions was

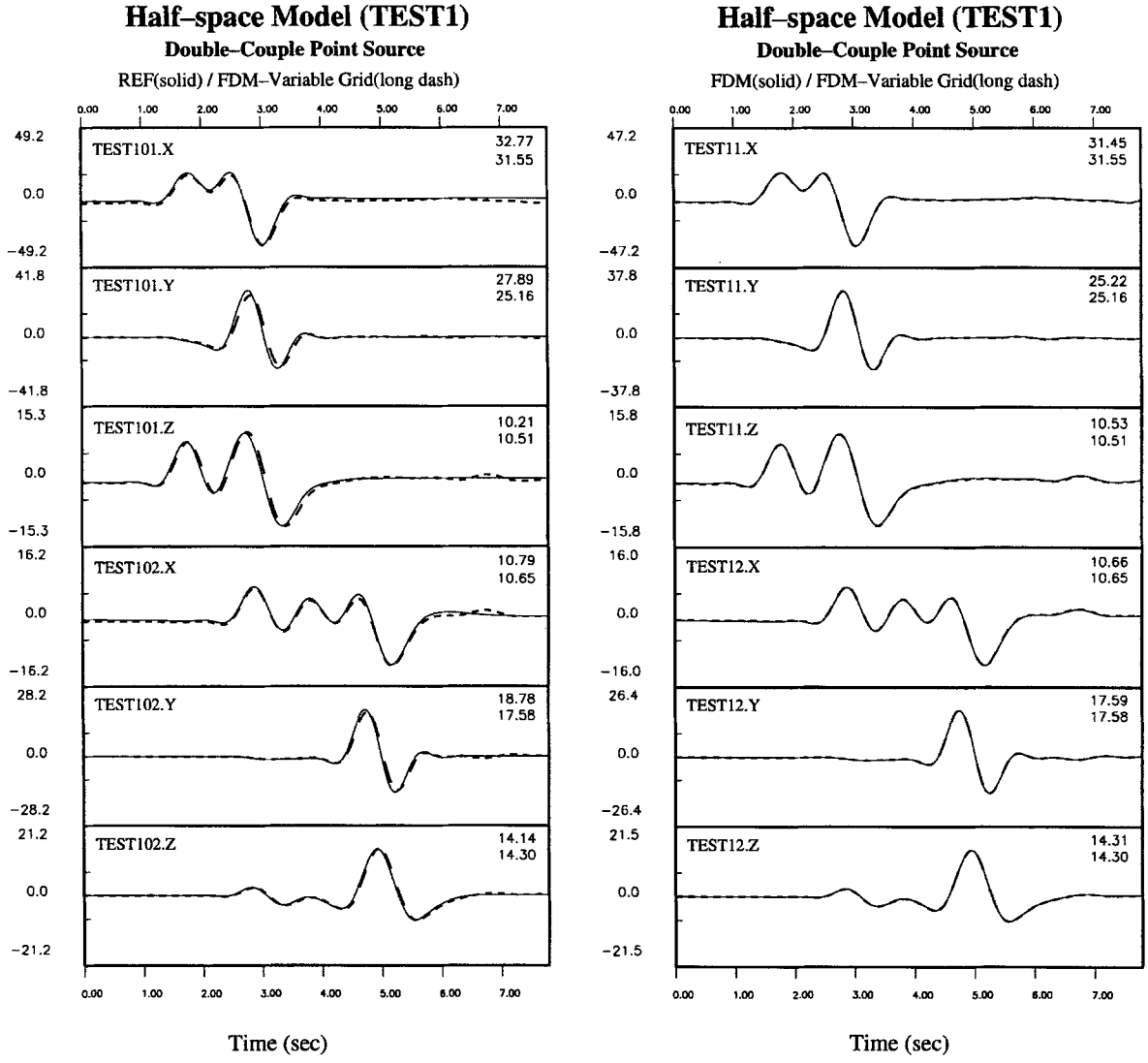


Figure 5. Comparison of three-component synthetic velocity seismograms calculated with the 3D-FD method with vertically nonuniform grid spacing (*dotted line*) and reflectivity method (*solid line, left panel*), as well as the 3D-FD method with uniform-grid spacing (*solid line, right panel*), at receivers 1 and 2 for a double-couple point source and model TEST1. Peak velocity is indicated on the left of each seismogram.

constant 0.125 km. With this variable grid spacing, the model has approximately 6 and 12 grid points per shear wavelength, respectively, in the lower and upper regions of the model at the upper frequency limit of 1.5 Hz. The velocity seismograms calculated with the nonuniform-grid FD technique are compared with those obtained with the reflectivity (REF) technique (Fig. 5, left panel) and uniform-grid FD technique with constant grid spacing of 0.125 km (Fig. 5, right panel). The synthetics are bandpass filtered at 0.1 to 1.5 Hz. The agreement among the three techniques is very good. Note that the FD calculations with uniform- and nonuniform-grid spacing give essentially identical results.

In the TEST2 model (Fig. 4, middle panel), I added a soft thin layer at the top of the half-space and increased the vertical grid spacing ratio between the two regions up to a factor of 3, the grid spacing in the lower region being 0.375 km. This ratio is proportional to that of shear-wave velocity ratio of the surface layer and the half-space. The grid spacing in the upper region and in the two horizontal directions was 0.125 km. The velocity seismograms calculated with the nonuniform FD technique are compared with those obtained with REF at an observation point located on the free surface at the horizontal range of 10 km (Fig. 6). The synthetic seismograms are bandpass filtered between 0.1 and 1.3 Hz. The upper frequency limit was defined assuming a minimum of 6 grid points per shear wavelength in the vertical direction. Again the agreement between the two techniques is very good, suggesting that the FD scheme with nonuniform grid spacing can handle models with strong velocity contrast.

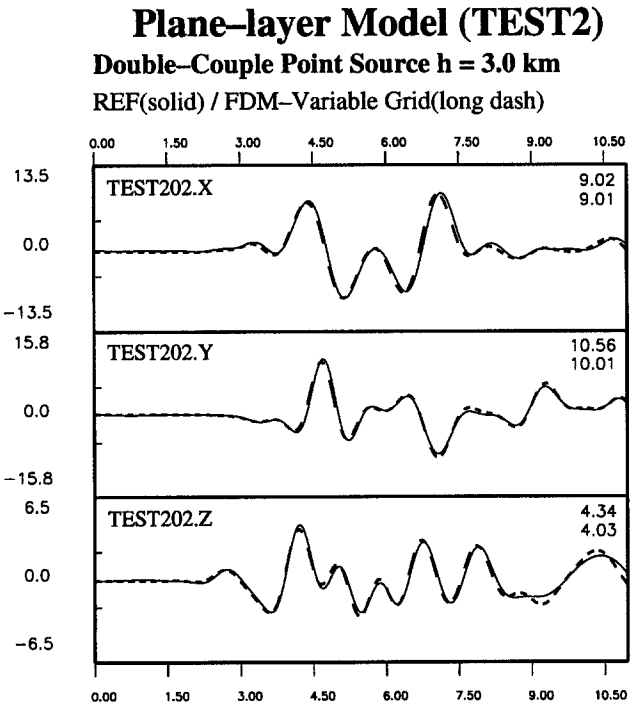


Figure 6. Same as the left panel of Figure 5 except for the velocity model TEST2.

In some applications of 3D-FD modeling, we are interested in studying the response of surface sediments for very shallow sources. Shallow sources are efficient at exciting surface waves in such media. The surface waves remain trapped inside the softer surface layers developing complicated waveforms with relatively large amplitudes. Model TEST3 (Fig. 4, right panel) was designed to test the capability of the new scheme to handle this situation. The source was located at four grid spacings below the free surface at a depth of 0.5 km. The 3D grid is the same as the one used in the TEST2 model. The comparison between the FD and REF synthetics bandpass filtered between 0.1 and 1.3 Hz is shown in Figure 7. The techniques produce results that are in good agreement.

I have tested the performance of the nonuniform-grid FD scheme using 1D velocity models, and with the grid spacing being variable only in the vertical direction. Next I extended the analysis to a basin model with a strong velocity contrast between the basin and the bedrock (Table 2) and used a grid spacing that is nonuniform in both horizontal and vertical directions. The semi-ellipsoidal basin, hypocenter, and computational region are shown in Figure 8. I divided the 3D grid into two regions with different grid spacings. The grid spacing is 0.1 km in the inner region, which includes the basin, and 0.4 km in the outer region. The grid spacing in each of the two regions was defined so as to satisfy the criteria of having 6 grid points per shear wavelength everywhere in the model. The grid spacing contrast between the two regions replicates the shear-wave velocity contrast between the basin and the bedrock. The region with the refined grid was intentionally extended up to three of the six edges of the model space, including the free surface.

The result of the test is shown in Figure 9, which compares synthetic velocity seismograms calculated with both the constant and varying grid spacings for a double-couple point source (strike = 30°, dip = 90°, rake = 30°), seismic moment $M_o = 10^{25}$ dyne cm, and a bell-shaped source-time function with a duration of 0.8 sec. The source is located at a depth of 10 km. The accuracy of the two techniques is expected to be the same in the frequency range 0.1 to 1.3 Hz because the smallest grid spacing in the basin is the same in both calculations. The bandpass filtered (0.1 to 1.3 Hz) velocity seismograms are calculated at receivers located on the free surface along a line across the basin. The synthetics obtained by the two techniques are very close. Because the nonuniform-grid calculation required about 6 times less computer core memory than that with the uniform grid and the time increment was the same, the computation time was reduced by a factor of 6. The improvement in computational memory is model dependent, but for sedimentary basin structures with low velocity, the gain is considerable in most cases.

Figure 10 compares the peak velocity patterns calculated with the two techniques. A logarithmic scaling of amplitudes is used in order to enhance the small amplitudes of waves propagating in the area outside the basin. As expected

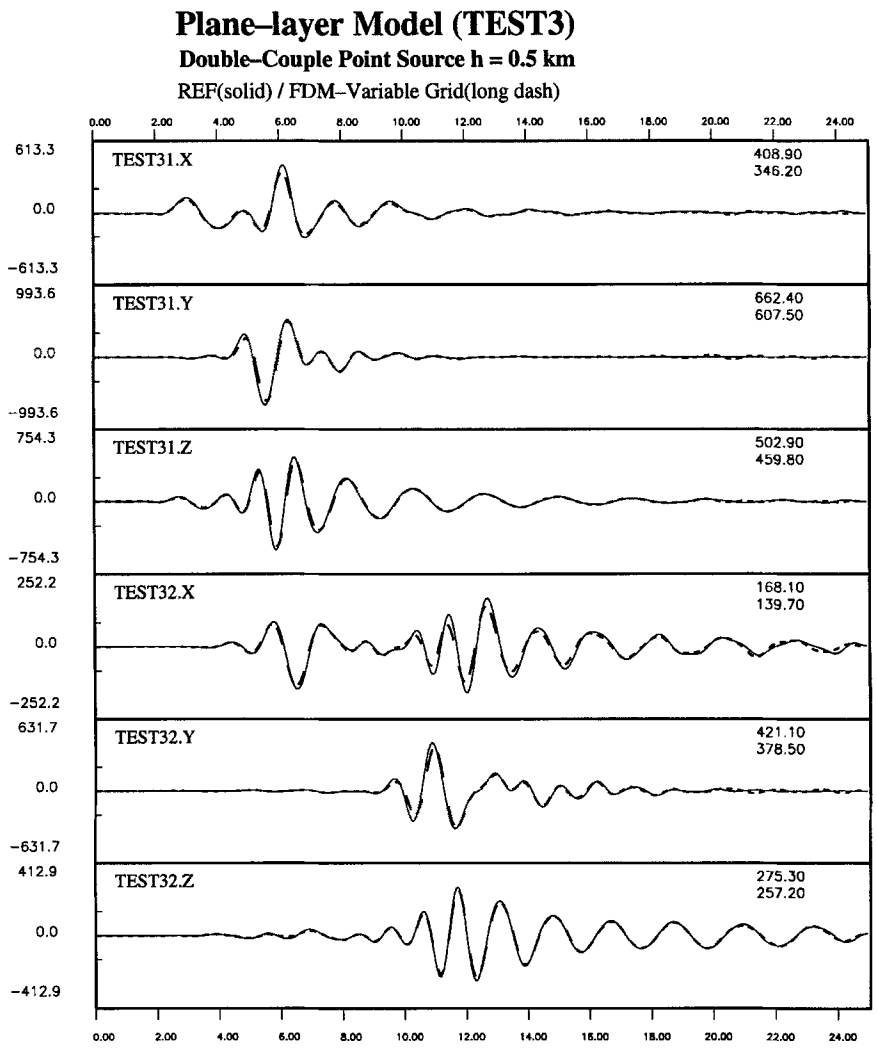


Figure 7. Same as the left panel of Figure 5 except for the velocity model TEST3.

Table 2
Model TEST4

| | $V_p$ (km/sec) | $V_s$ (km/sec) | $\rho$ (g/cm$^3$) |
|---|---|---|---|
| Basin Layer | 1.9 | 0.8 | 2.0 |
| Bedrock | 5.6 | 3.2 | 2.2 |

from the very good agreement in the waveforms, the agreement of the peak velocity distribution between the two techniques is very good. There is no noticeable distortion of the incident and scattered waves as they propagate through the boundary between the two regions with different grid spacings, including the free surface, even though the grid spacing contrast between the two regions is a factor of 4.

When the difference in adjacent grid intervals becomes large, it is conceivable that the accuracy of the finite-difference operators decreases. Such cases should be avoided by using gradually varying grid increments. The result obtained with the basin model demonstrates that grid increments of four are appropriate.

## Source Implementation Tests

The implementation of a double-couple point source into 3D finite-difference grid using either particle velocity components or stress components at a source has been demonstrated to be accurate. Based on an appropriate distribution of equivalent body forces, Graves (1996b) modified Frankel's approach (Frankel, 1993) for the velocity-stress scheme on a staggered grid. In the case of the staggered grid with variable grid spacing, the stress approach described by equation (15) is easier to implement. Moreover, it reduces the asymmetry in the source excitation caused by the staggered grid.

To assess the accuracy of the stress approach in the nonuniform FD technique, I performed calculations for the extreme case where the grid spacing varies in the source

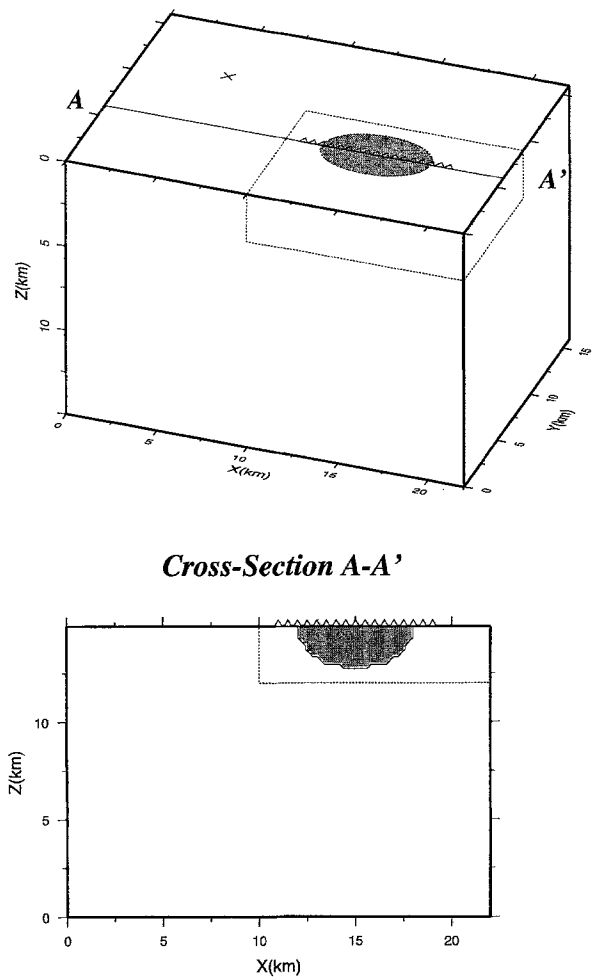


Figure 8. Velocity Model TEST4: half-ellipsoid basin structure embedded in a homogeneous half-space. The boundary between fine- and coarse-grid zones is indicated by dotted lines. Triangles indicate the receiver locations, and the cross indicates the epicenter location of a double couple at a depth of 10 km.

region. Such a case may be encountered in modeling ground motions for both a double-couple point source or an extended fault.

Double-Couple Point Source

In the following analysis, I compare double-couple point source seismograms calculated analytically (Aki and Richards, 1980, p. 81) with those obtained using the proposed FD technique with nonuniform- and uniform-grid spacings of 0.1 km. In the nonuniform grid, grid spacings around the source region are 0.1, 0.2, and 0.3 km along the $x$, $y$, and $z$ directions, respectively. The source is located in an unbounded homogeneous medium ($v_p$ = 4.0 km/sec, $v_s$ = 2.3 km/sec, $\rho$ = 1.8 gm/cm$^3$). The calculations at two receivers located at the same depth as the source are performed for a double-couple point source (strike = 30°, dip = 80°, rake = 30°) and a seismic moment of $M_0 = 10^{24}$ dyne cm. The location of the two receivers is given in Table 3. For all calculations, a 1-sec bell-shaped source-time function was used, and the response has been bandpass filtered at 0.1 to 1.2 Hz. At the upper frequency limit of 1.2 Hz, the variable grid has the minimum of 6 grid points per shear-wave wavelength while the constant grid has 19 grid points.

Figure 11 compares analytical velocity seismograms with those computed by the nonuniform (left panel) and uniform (right panel) grid FD technique at the two receivers. The agreement between the analytical response and the one calculated with the nonuniform grid is very good both in terms of amplitude and waveform. It is clear that the technique used in this study to incorporate the source into the grid with nonuniform-grid spacing works as well as the uniform-grid technique. The result of this test also shows that the source formulation based on the stress components accurately represents the double-couple point source.

Finite-Fault Representation

The response to heterogeneous rupture along a finite fault can be calculated using a distribution of moment tensor point sources. Point sources are usually distributed regularly in the grid on an interface corresponding to the fault surface. In order to accurately represent rupture process on a finite fault, the point source spacing should be on the order of the shortest wavelength or less. This condition can be easily satisfied by both uniform- and nonuniform-grid FD schemes because the grid spacing is defined based on the accuracy condition that requires that the grid spacing should be at least five times smaller than the shortest wavelength (e.g., Levander, 1988).

The calculation of the finite-fault response with the nonuniform-grid finite-difference method is performed using irregular distribution of point sources. In order to assess how much the irregularity in the point source distribution affects the modeling of such rupture process, I computed the response of a finite fault using both uniform- and nonuniform-grid FD techniques.

I considered the rupture on a 10-km-long planar vertical fault that extends from a depth of 2 to 10 km. The slip model was constructed using a random slip distribution with the rake angle of the slip vector in each subfault constrained between $-6°$ and 60° (Fig. 12). The model allows slip to occur in a single time window with a 1-sec time duration. I used a bell-shaped slip velocity function and the constant rupture velocity of 2.8 km/sec. The fault-receiver geometry is shown in Figure 13.

In the uniform-grid computation, the interval of point sources and the grid spacing were set to 0.2 and 0.1 km (Fig. 12a) respectively. In the nonuniform-grid computation, the grid spacing was set to 0.1 km in the $x$ and $y$ directions and 0.1, 0.3, and 0.6 in the $z$ direction in the depth intervals of 0 to 4.0, 4.0 to 8.0, and 8 to 14.0 km, respectively. In these depth intervals, the point source spacing in the vertical direction was set to 0.2, 0.3, and 0.6, respectively (Fig. 12b).

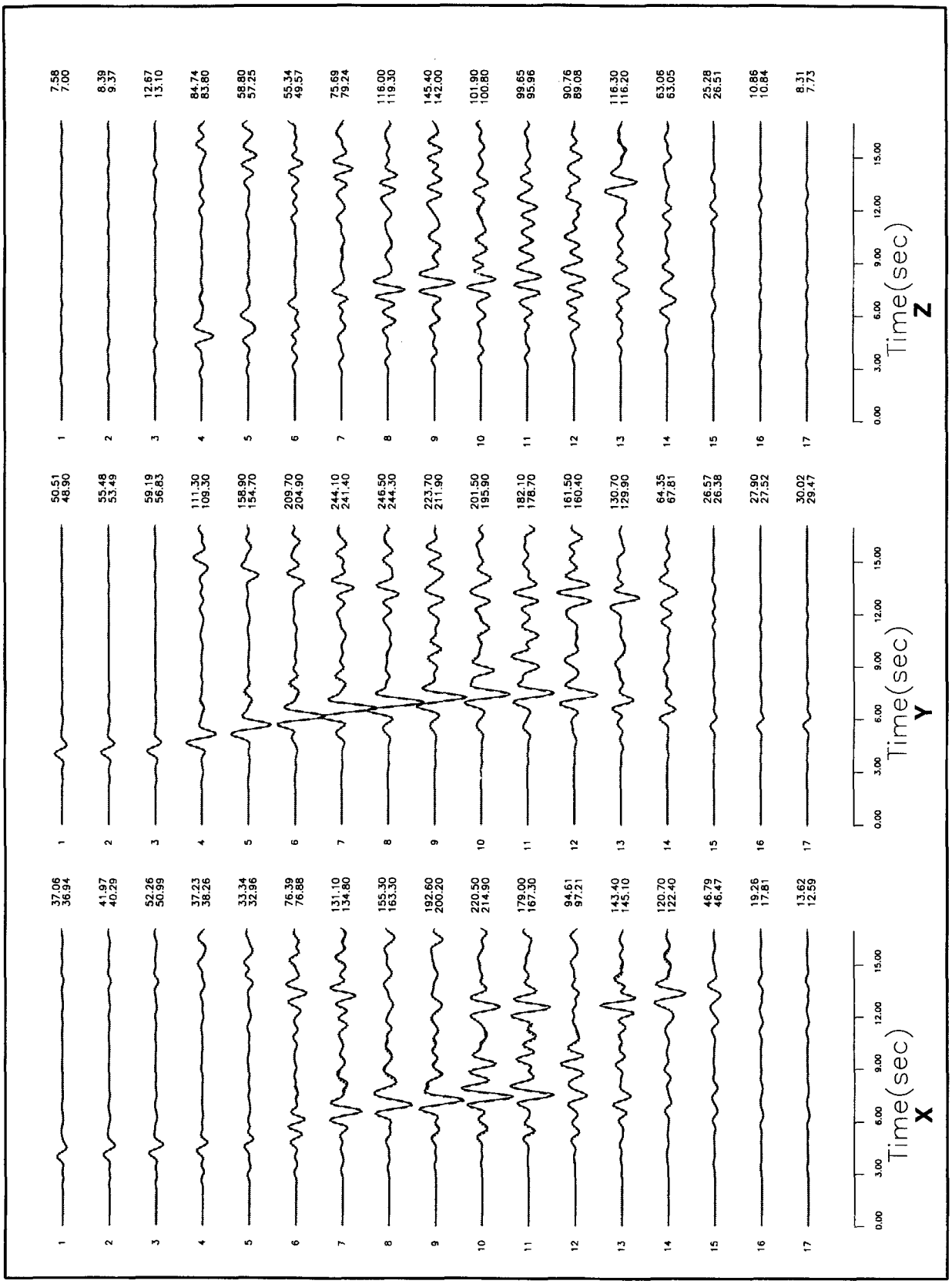


Figure 9. Comparison of three-component velocity seismograms calculated with the nonuniform-grid spacing FD method (*dashed trace*) and the uniform-grid spacing FD method (*solid trace*) for the velocity structure TEST4. All seismograms are bandpass filtered at 0.1 to 1.3 Hz. Peak velocity is shown on the left of each seismogram.

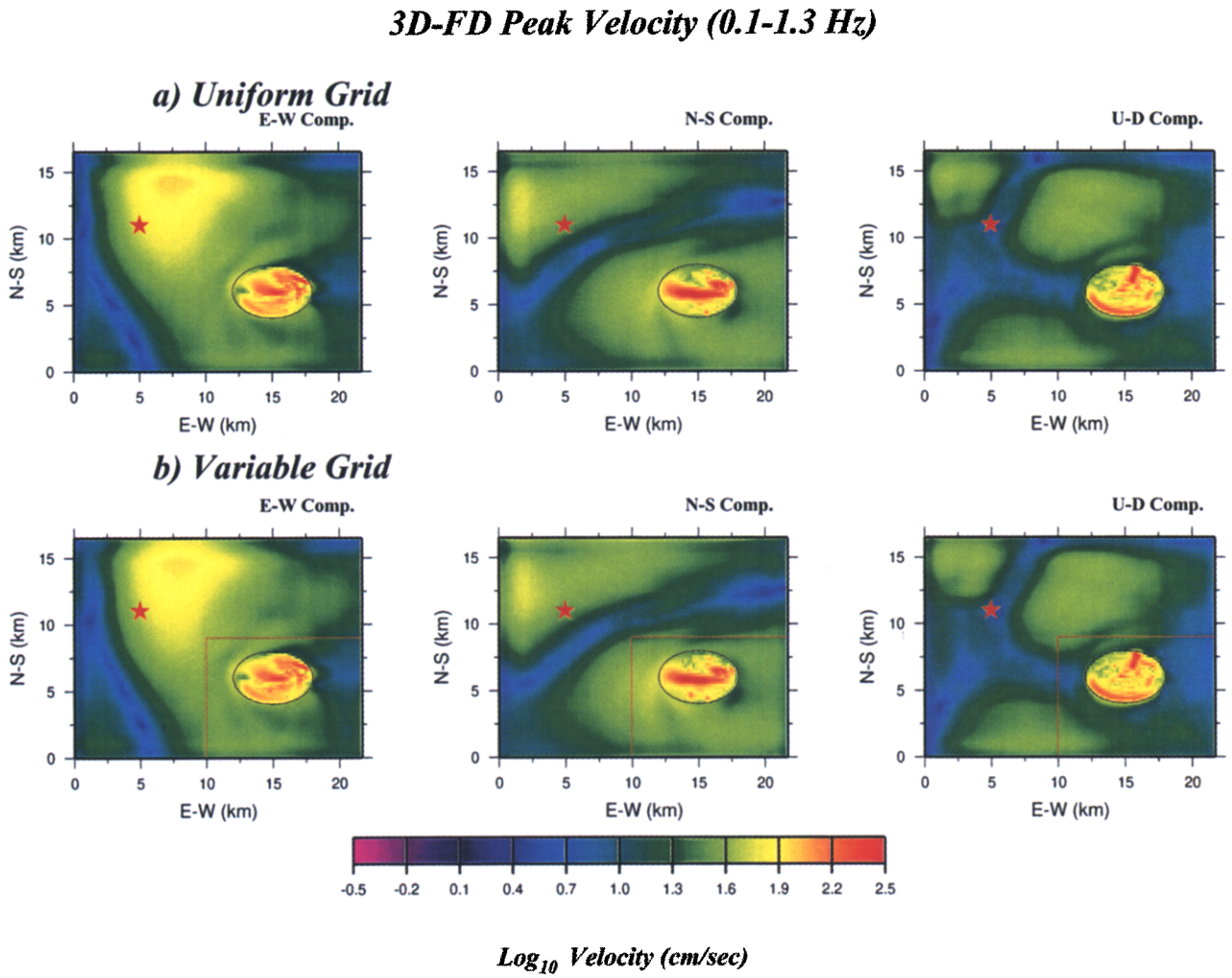


Figure 10. Comparison of the free-surface peak velocity ground motion calculated with the uniform-grid spacing FD method (*upper panel*) and the nonuniform-grid spacing FDM (*lower panel*) for TEST4. Star indicates the location of the source epicenter, and a red dotted line indicates the boundary between fine and sparse grid zones.

Table 3
Station Locations

| Station Name | Azim (°) | Range (km) |
|---|---|---|
| sta1 | 26.56 | 2.18 |
| sta2 | 45.00 | 2.76 |

In both models, the largest point source spacing is smaller than the shortest wavelength computed. For these calculations, I used a homogeneous half-space model ($v_p$ = 5.6 km/sec, $v_s$ = 3.2 km/sec, $\rho$ = 2.2 gm/cm$^3$).

The comparison of synthetic velocity seismograms at near-fault receivers calculated with the uniform- and nonuniform-grid techniques is shown in Figure 14. Very good agreement between both synthetics shows the validity of the nonuniform FD method at modeling the response of the present finite fault. The reduction in computer memory and computation time in this simple test model obtained with the variable grid-spacing technique is a factor of 2.2. This result also demonstrates that the fault representation by an irregular distribution of point sources with the source spacing smaller than the shortest wavelength does not adversely affect the calculated fault response.

## Conclusions

The frequency band of waves modeled with any finite-difference scheme represents a trade-off between the size of models and computer resources. Besides the memory opti-

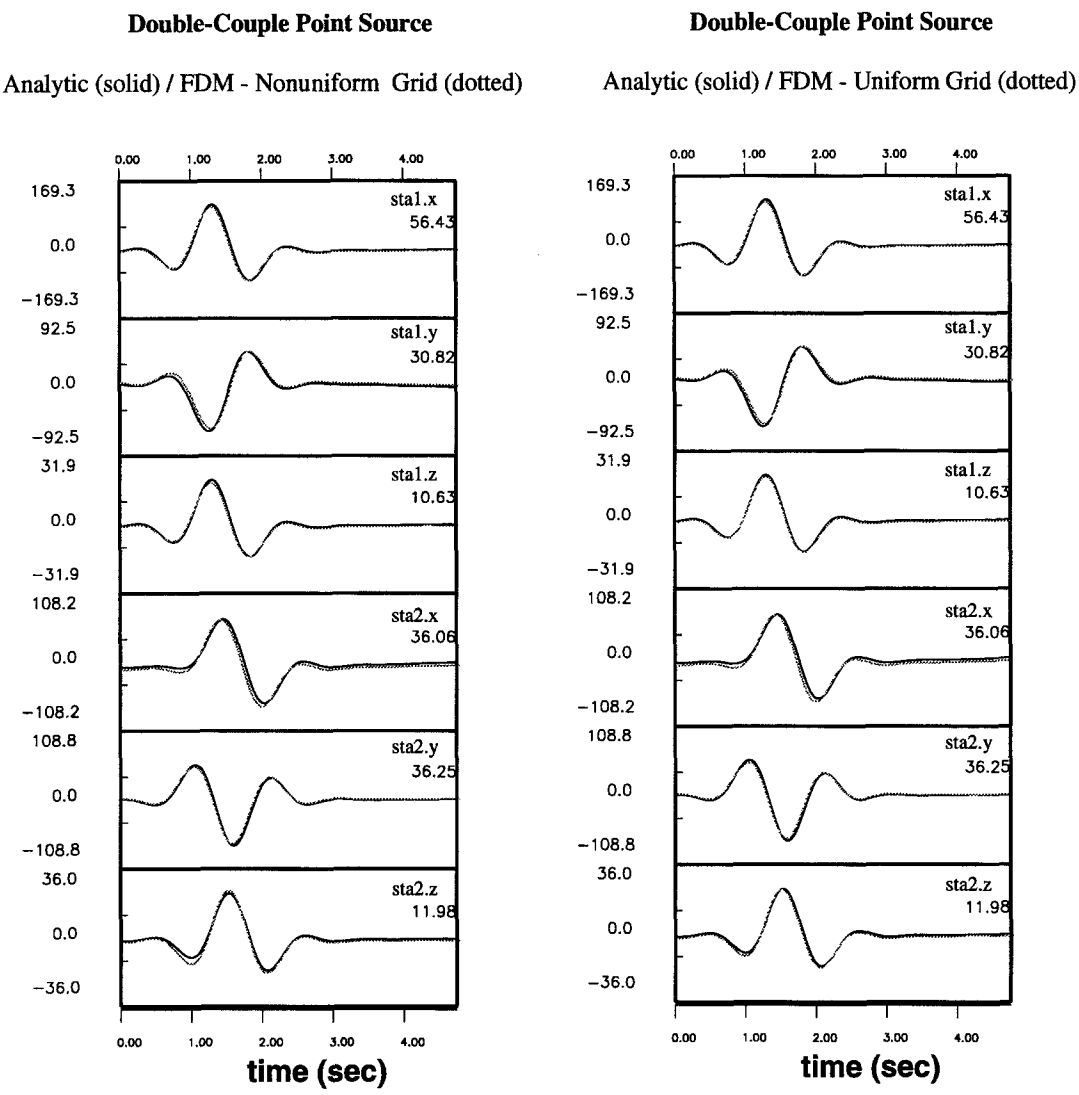


Figure 11. Comparison between the analytic solution of 3D elastic-wave equation (*solid trace*) and three-component synthetic velocity seismograms calculated with 3D-FD method with vertically nonuniform-grid spacing (*dotted trace, left panel*) and 3D-FD method with uniform grid spacing (*dotted trace, right panel*) at two receivers for a double-couple point source and homogeneous full-space velocity model. Peak velocity is shown on the left of each seismogram.

mization technique (Graves, 1996), an attractive way of reducing the computational requirement is to adjust the grid spacing depending on the velocity inside each model. The use of the grid system with nonuniform spacing results in a considerable reduction of computer memory requirement and computation time.

In this study, I have used the staggered-grid finite-difference formulation to solve the elastic wave equation. The formulation involves only first-order derivatives of velocity and stress components. This property makes the staggered-grid scheme attractive, especially when it is applied to the grid with nonuniform spacing. I showed how to derive the derivative operators of fourth-order accuracy and their explicit expressions used in a variable staggered-grid 3D elastic media with the finite-difference method.

Some numerical tests in this study demonstrate that the proposed nonuniform staggered-grid finite-difference formulation is efficient and sufficiently accurate at modeling wave propagations in 3D elastic media. The accuracy and stability conditions are locally the same as in the uniform staggered-grid scheme. All the numerical tests were performed with a minimum of 6 grid spacings per shortest shear wavelength. Up to four grid increments did not affect the accuracy of the results.

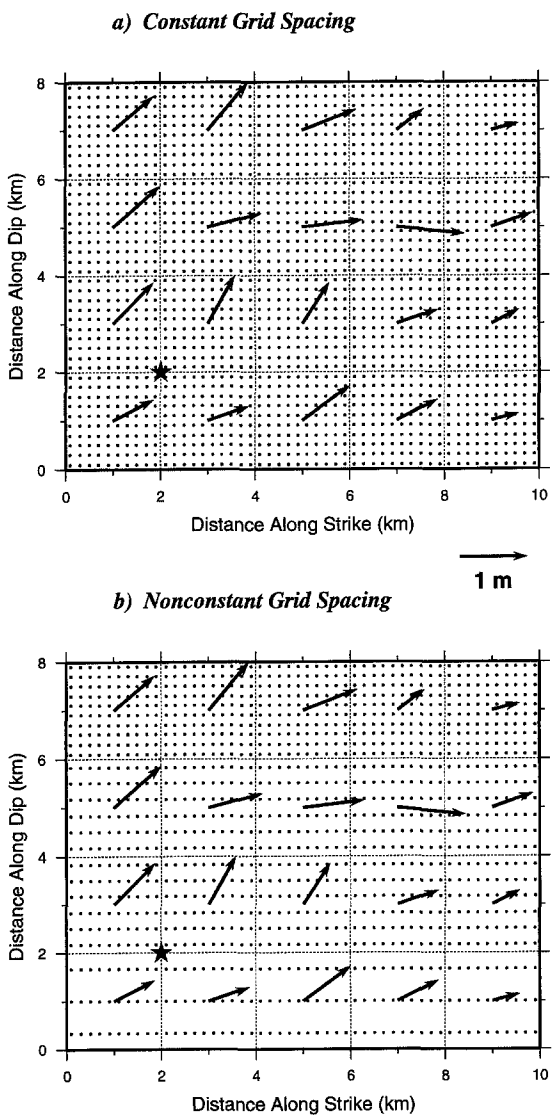


Figure 12. Slip vector and point source distribution on a vertical fault. (a) Uniform grid and (b) nonuniform grid.

The method significantly decreases the computational requirement of the 3D finite-difference modeling in realistic large-scale geological structures.

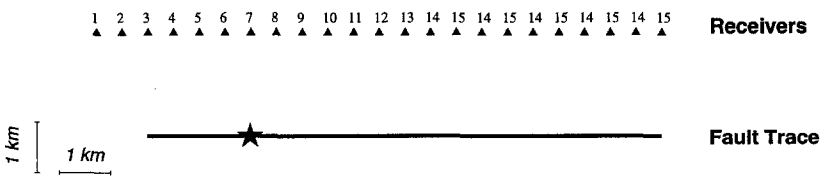


Plan View

Figure 13. Fault receiver configuration. Star indicates the location of the rupture initiation point.

## Acknowledgments

Discussions with Robert Graves, Kojiro Irikura, and Paul Somerville during the course of this study provided valuable insight. I thank Hiroshi Takenaka (Kyushu University), Japan, for providing his reflectivity code and Jorge Pita for the information on his 3D-FD technique. Two anonymous reviewers made valuable suggestions to improve the article. This research was sponsored by USGS Grant Number 1434-HQ-98-GR-00032.

## References

Aki, K. and P. G. Richards (1980). *Quantitative Seismology,* W.H. Freeman and Company, San Francisco.

Aoi, S. and H. Fujiwara (1997). 3D seismic wave simulation using finite-difference method with discontinuous grid, *EOS* **78,** F424.

Clayton, R. W. and B. Engquist (1977) Absorbing boundary conditions for acoustic and elastic wave equations, *Bull. Seism. Soc. Am.* **67,** 1529–1540.

Coutant, O., J. Virieux, and A. Zollo (1995). Numerical source implementation in a 2D finite-difference scheme for wave propagation, *Bull. Seism. Soc. Am.* **85,** 1507–1512.

Falk J., E. Tessmer, and D. Gajewski (1996). Tube wave modeling by the finite-difference method with varying grid spacing, *Pageoph* **148,** 77–93.

Frankel, A. (1993). Three-dimensional simulations of ground motions in the San Bernardino Valley, California, for hypothetical earthquakes on the San Andreas Fault, *Bull. Seism. Soc. Am.* **83,** 1042–1063.

Frankel, A. and J. Vidale (1992). A three-dimensional simulation of seismic waves in the Santa Clara Valley, California, from a Loma Prieta aftershock, *Bull. Seism. Soc. Am.* **82,** 2045–2074.

Graves, R. W. (1993). Modeling three-dimensional site response in the Marina District basin, San Francisco, California, *Bull. Seism. Soc. Am.* **83,** 1042–1063.

Graves, R. W. (1996a). Simulating realistic earthquake ground motions in regions of deep sedimentary basins, *Proc. of the 11th World Conference on Earthquake Engineering,* Acapulco, Mexico, June 23–28, 1996.

Graves, R. W. (1996b). Simulating seismic wave propagation in 3D elastic media using staggered-grid finite-differences, *Bull. Seism. Soc. Am.* **86,** 1091–1107.

Graves, R. W. (1998). Three-dimensional finite-difference modeling of the San Andreas fault: source parameterization and ground motion levels, *Bull. Seism. Soc. Am.* **88,** 891–897.

Jastram C. and A. Behle (1992). Acoustic modeling on a grid of vertically varying spacing, *Geophys. Prospecting* **40,** 157–169.

Jastram, C. and E. Tessmer (1994). Elastic modelling on a grid with vertically varying spacing, *Geophys. Prospecting* **42,** 357–370.

Levander, A. R. (1988). Fourth-order finite-difference P-SV seismograms, *Geophysics* **53,** 1425–1436.

Miyatake, T. (1980). Numerical Simulations of earthquake source process by a three-dimensional crack model. Part I. Rupture process (1980). *J. Phys. Earth* **28,** 565–598.

Moczo, P. (1989). Finite-difference technique for SH-wave in 2-D media

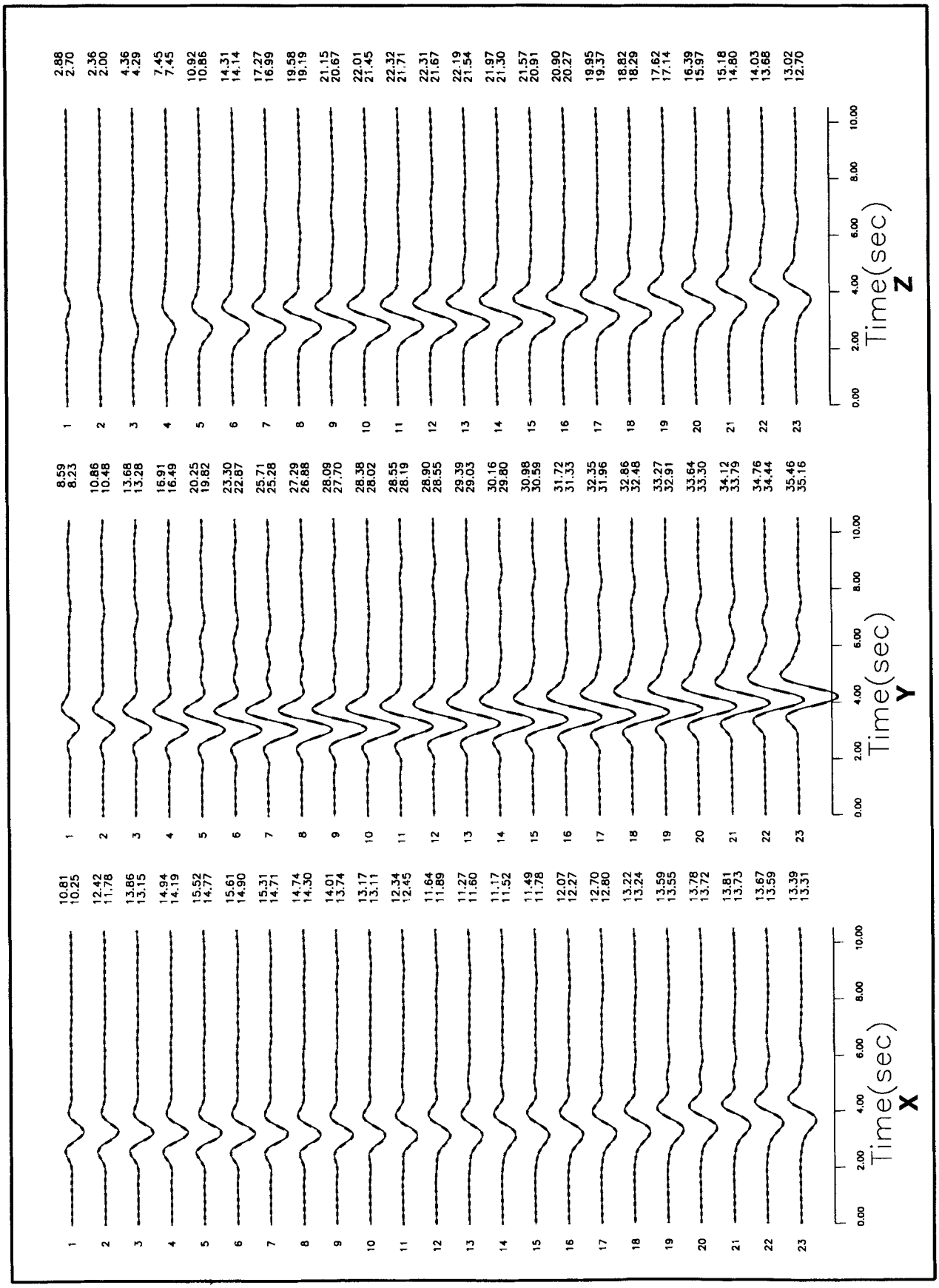


Figure 14. Same as Figure 9 except for the slip model in Figure 12.

using irregular grids—application to the seismic response problem, *Geophys. J. Int.* **99,** 321–329.

Moczo, P. Labák, J. Kristek, and F. Hron (1996). Amplification and differential motion due to an antiplane 2D resonance in the sediment valleys embedded in a layer over the half-space, *Bull. Seism. Soc. Am.* **86,** 1434–1446.

Moczo, P., E. Bystricky, J. Kristek, J. M. Carcione, and M. Bouchon (1997). Hybrid modeling of P-SV seismic motion at inhomogeneous viscoelastic topographic structures, *Bull. Seism. Soc. Am.* **87,** 1305–1323.

Mufti, R. I., J. A. Pita, and R. Huntley (1996). Finite-difference depth migration of exploration-scale 3-D seismic data, *Geophysics* **61,** 776–794.

Ohminato, T. and B. A. Chouet (1997). A free-surface boundary condition for including 3D topography in the finite-difference method, *Bull. Seism. Soc. Am.* **87,** 494–515.

Olsen, K. B. and R. J. Archuleta (1996). 3-D simulation of earthquakes on the Los Angeles fault system, *Bull. Seism. Soc. Am.* **86,** 575–596.

Olsen, K. B., R. J. Archuleta, and J. R. Matarese (1995). Magnitude 7.7 earthquake on the San Andreas fault: three-dimensional ground motion in Los Angeles, *Science* **270,** 1628–1632.

Pitarka, A. and K. Irikura (1996). Modeling 3-D surface topography by finite-difference method: the Kobe JMA station site case study, *Geophys. Res. Lett.* **23,** 2723–2732.

Pitarka, A., K. Irikura, T. Iwata, and H. Sekiguchi (1998). Three-dimensional simulation of the near-fault ground motion for the 1995 Hyogoken Nanbu (Kobe), Japan, earthquake, *Bull. Seism. Soc. Am.* **88,** 428–440.

Virieux, J. (1986). P-SV wave propagation in heterogeneous media: velocity-stress finite-difference method, *Geophysics* **51,** 889–901.

Wald, D. J. and R. W. Graves (1998). The seismic response of the Los Angeles Basin, California, *Bull. Seism. Soc. Am.* **88,** 337–356.

Yomogida, K. and J. T. Etgen (1993). 3-D wave propagation in the Los Angeles Basin for the Whittier-Narrows earthquake, *Bull. Seism. Soc. Am.* **83,** 1325–1344.

Yuan, Y., Y. Shizou, and Y. Osawa (1986). Strong ground motion simulation of the 1976 Ninghe, China earthquake, *Bull. Earthquake Res. Inst. Univ. Tokyo* **61,** 97–127.

URS Greiner Woodward Clyde
Federal Services
566 El Dorado Street, Suite 100
Pasadena, California 91101
E-mail: axpitar0@wcc.com

Manuscript received 12 May 1998.